

ARTICLE

High-quality genome-scale metabolic model of *Aurantiochytrium* sp. T66

Vetle Simensen¹  | André Voigt¹  | Eivind Almaas^{1,2} 

¹Department of Biotechnology and Food Science, NTNU - Norwegian University of Science and Technology, Trondheim, Norway

²Department of Public Health and General Practice, K.G. Jebsen Center for Genetic Epidemiology, NTNU - Norwegian University of Science and Technology, Trondheim, Norway

Correspondence

Eivind Almaas, Department of Biotechnology and Food Science, NTNU - Norwegian University, of Science and Technology, N-7491 Trondheim, Norway.
Email: eivind.almaas@ntnu.no

Funding information

The Norwegian Research Council, BIOTEK2021, Grant/Award Number: 269432

Abstract

The long-chain, ω -3 polyunsaturated fatty acids (PUFAs) (e.g., eicosapentaenoic acid [EPA] and docosahexaenoic acid [DHA]), are essential for humans and animals, including marine fish species. Presently, the primary source of these PUFAs is fish oils. As the global production of fish oils appears to be reaching its limits, alternative sources of high-quality ω -3 PUFAs is paramount to support the growing aquaculture industry. Thraustochytrids are a group of heterotrophic protists with the capability to synthesize and accrue large amounts of DHA. Thus, the thraustochytrids are prime candidates to solve the increasing demand for ω -3 PUFAs using microbial cell factories. However, a systems-level understanding of their metabolic shift from cellular growth into lipid accumulation is, to a large extent, unclear. Here, we reconstructed a high-quality genome-scale metabolic model of the thraustochytrid *Aurantiochytrium* sp. T66 termed iVS1191. Through iterative rounds of model refinement and extensive manual curation, we significantly enhanced the metabolic scope and coverage of the reconstruction from that of previously published models, making considerable improvements with stoichiometric consistency, metabolic connectivity, and model annotations. We show that iVS1191 is highly consistent with experimental growth data, reproducing in vivo growth phenotypes as well as specific growth rates on minimal carbon media. The availability of iVS1191 provides a solid framework for further developing our understanding of T66's metabolic properties, as well as exploring metabolic engineering and process-optimization strategies in silico for increased ω -3 PUFA production.

KEYWORDS

Aurantiochytrium sp. T66, genome-scale model, lipid-producing cell factories, thraustochytrids, ω -3 PUFAs

1 | INTRODUCTION

The health benefits from the consumption of marine seafood are well documented (Bloomer et al., 2009; Bouwens et al., 2009; Coletta et al., 2010; Hosomi et al., 2012; Lauritzen et al., 2016). The high content of ω -3 polyunsaturated fatty acids (PUFAs), such as

docosahexaenoic acid (DHA), is considered one of the major contributors to this effect (Hosomi et al., 2012; Swanson et al., 2012). Although rich in ω -3 fatty acids, oily fish such as salmon do not synthesize these de novo, instead acquiring them by feeding on lipid-rich plankton and microalgae (Hosomi et al., 2012). The rising global aquaculture industry has consequently led to an increasing need for

This is an open access article under the terms of the Creative Commons Attribution-NonCommercial License, which permits use, distribution and reproduction in any medium, provided the original work is properly cited and is not used for commercial purposes.

© 2021 The Authors. *Biotechnology and Bioengineering* published by Wiley Periodicals LLC.

novel sources of these fatty acids (Food and Agriculture Organization of the United Nations, 2018), the current source of which is mainly fish oil. These PUFA-containing lipids, however, also contain elevated levels of toxic contaminants, such as polychlorinated biphenyls and heavy metals (El-Moselhy et al., 2014; Rawn et al., 2006). A need for alternative, clean, high-quality sources of ω -3 PUFAs is therefore of utmost importance. Cultivation and strain engineering of lipid-producing microorganisms is regarded as a promising strategy to cater to this demand. These oleaginous organisms are able to accumulate substantial amounts of lipids and has proven to be a cost-effective alternative to agricultural oil production (Ratledge, 2004). Thraustochytrids are heterotrophic protists found globally in marine and estuarine environments (Leyland et al., 2017). They accrue large quantities of ω -3-rich triacylglycerols (TAGs) that may constitute 50%–80% of the total cell mass (Huang et al., 2012; Leyland et al., 2017; Li et al., 2015). In most PUFA-producing microorganisms, the fatty acids are produced by elongating and desaturating the end products of the type I fatty acid synthase (FAS) enzymatic machinery (Beld et al., 2015). However, thraustochytrids predominately synthesize their PUFAs using a competing polyketide synthase-like (PKS) system (Metz et al., 2001). Here, the acyl intermediates may retain their unsaturated bonds during the biosynthetic process, thus lowering the molar requirement for reducing power compared with the conventional elongation/desaturation scheme. This capability to accumulate large amounts of ω -3 PUFAs, as well as the decreased biosynthetic requirement for reducing power, has made thraustochytrids particularly promising candidates as efficient lipid-producing cell factories (Ratledge, 2004).

To elucidate the biological mechanisms underpinning the fatty acid biosynthesis and lipid accumulation in thraustochytrids, knowledge of their global metabolic organization and functionality is vital. Metabolic modeling is a pivotal methodology to simulate and predict metabolic phenotypes *in silico*, thereby generating hypotheses and guide experimental efforts (O'Brien et al., 2015). Specifically, genome-scale metabolic models (GSMs) have become one of the main approaches to model metabolism within the field of systems biology (Gu et al., 2019). Whereas some modeling approaches require extensive parametrization, constraint-based modeling using GSMs in their most fundamental form merely calls for an annotated genome sequence (Thiele & Palsson, 2010). GSMs contain the genotype–phenotype relationships for genes and biochemical reactions, enabling the computational simulations of metabolic flux distributions under various environmental and genetic perturbations (O'Brien et al., 2015).

GSMs have been constructed for a wide variety of oleaginous microorganisms, providing novel insight into their metabolic capabilities and behavior (Castañeda et al., 2018; Kim et al., 2019; Levering et al., 2015; Loira et al., 2012; Mishra et al., 2016; Tiukova et al., 2019; Vongsangnak et al., 2013). Many of these GSMs have also been used to propose strategies to enhance both the total lipid content, as well as increasing the fractional PUFA-content (Kim et al., 2019; Levering et al., 2015; Tibocha-Bonilla et al., 2018). These models, however, have predominately focused on oleaginous yeast

and lipid-producing phototrophic microalgae. Presently, only two thraustochytrid GSMs have been reconstructed. The first reconstruction, iCY1170_DHA, is of one of the more studied thraustochytrid strains *Schizochytrium limacinum* SR21 (Ye, Qiao, et al., 2015). Ye, Qiao, et al. (2015) built the GSM using three existing models, refining the reconstruction by predicting its subcellular compartmentalization and performing appropriate model curations. They also proposed multiple cultivation and strain engineering strategies for increasing the DHA productivity. The second model was of *Oblongichytrium* sp. RT2316-13, reconstructed by modifying iCY1170_DHA to reflect the metabolism of RT2316-13 (Shene et al., 2020). This GSM was used in combination with an auxiliary mathematical model to simulate the fermentation profile of batch cultures, showing satisfactory agreements with experimental data. The model was further able to predict the effects of oxygen availability on the rate of lipid synthesis.

The process of GSM reconstruction is a labor-intensive endeavor that is based on the prediction of putative metabolic functions of protein-encoding sequences using the aforementioned genome annotation (Mendoza et al., 2019). Once collected, this repository of biochemical reactions and metabolites are converted into the mathematical framework of a stoichiometric matrix, enabling the simulation of metabolic phenotypes using flux balance analysis (FBA) and related approaches (Bordbar et al., 2014). Although consecutive in order, these stages are organized in an iterative manner in which additional model curation is performed to ensure that the predictions progressively match the expected biochemical phenotype (Thiele & Palsson, 2010). While manual curation is an integral part of achieving a high-quality GSM (Mendoza et al., 2019), many of the steps are included in fully automated software producing ready-to-use metabolic reconstructions (Agren et al., 2013; Dias et al., 2015; Henry et al., 2010; Karp et al., 2016; Machado et al., 2018; Pitkänen et al., 2014).

Herein, we present iVS1191, the reconstruction of a high-quality GSM of the thraustochytrid *Aurantiochytrium* sp. strain T66 (Jakobsen et al., 2007). By comprehensively refining and curating the reconstruction, we significantly improved the metabolic scope and coverage from that of a template model. We further utilized experimental growth data, proving the model able to accurately reproduce *in vivo* metabolic growth phenotypes. Currently, iVS1191 represents the most comprehensive knowledge-base of any thraustochytrid, and we strongly believe that the reconstructed model has the potential to play a key role in understanding the oleaginous metabolism of thraustochytrids for future biotechnological applications.

2 | MATERIALS AND METHODS

2.1 | Model simulations

We use FBA to predict cellular phenotypes of the GSM. The general FBA problem can be stated as the following linear program:

$$\max z = \sum_{j=1}^n c_j v_j \quad (1)$$

$$\text{s. t. } \sum_{j=1}^n s_{ij} v_j = 0, \forall i \in M, \quad (2)$$

$$v_j^{lb} \leq v_j \leq v_j^{ub}, \forall j \in N, \quad (3)$$

where c_j is the objective function coefficient of reaction flux v_j defining the objective function z as a linear combination of the reaction fluxes. Equation (2) represents the homogeneous system of linear equations, while Equation (3) specifies the upper (v_j^{ub}) and lower (v_j^{lb}) bounds on the flux variables (Orth et al., 2010). Unless otherwise stated, all FBA simulations took the form as seen in Equations (1)–(3) where the flux of the biomass pseudoreaction was selected as the objective. Simulations were performed on a Macbook Pro 2018 with Matlab 2019b (MATLAB, 2019) using the The COnstraint-Based Reconstruction and Analysis toolbox (Heirendt et al., 2019) and the proprietary solver Gurobi version 8.1.1 (Gurobi Optimization, 2020).

2.2 | Initial draft reconstruction

We used the already published GSM iCY1170_DHA (Ye, Qiao, et al., 2015) of the closely related thraustochytrid *S. limacinum* SR21 as a starting template. As our next step, we performed a reciprocal protein Basic Local Alignment Search Tool (BLASTp) (Altschul et al., 1990) analysis using the RAVEN Toolbox (Agren et al., 2013) with the predicted protein sequences of the template and target organisms as input. The predicted protein sequences of T66 were accessed from Gene Expression Omnibus (GEO; Edgar et al., 2002), GEO Series accession number GSE134374, while the protein sequences of *S. limacinum* were obtained from the Joint Genome Institute Database (Institute, 2017). The resulting sequence similarities were subsequently used to infer putative homologs by bidirectional best hits using the following parameters: alignment length of at least 200, an E-value $< 10^{-30}$, and a minimum identity of 40%. We also performed additional identification of candidate homologs of proteins that were unable to satisfy these similarity criteria due to short sequence lengths. All reactions from the template model associated with the identified set of putative homologs were extracted to form the initial draft reconstruction. In addition, reactions annotated as spontaneous in the template model were also included in the draft model.

The semi-automatic gap-filling approach was carried out as follows: Using the biomass reactions from the template model; for every biomass precursor incapable of being produced using a carbon-limited defined medium (see Table S1), we studied the anabolic pathways responsible for their production in the Kyoto Encyclopedia of Genes and Genomes (KEGG) (Kanehisa & Goto, 2000) and MetaCyc (Kothari et al., 2013) databases to identify putative gap-filling candidates. We also utilized the software ModelExplorer (Martyushenko & Almaas, 2019) for visual and algorithmic inspection of the metabolic network to identify metabolic gaps and inconsistencies. Finally, we filled the remaining gaps by adding a minimal subset of all unincorporated template model reactions necessary for the model to generate biomass.

2.3 | Draft reconstruction improvement based on KEGG

We reconstructed a secondary draft model using the KEGG functionality of the RAVEN Toolbox (Agren et al., 2013). This method makes use of profile hidden Markov models (HMM) pre-trained on KEGG Orthologies (KO) in the KEGG database and attempts to assign these identifiers to significantly homologous genes from organism of interest. The associated KO reactions are collected and used to generate a draft reconstruction. We obtained the secondary draft model by querying the predicted protein sequences of T66 against a pre-trained profile HMM (Eukaryota, Identity: 100%) from Ref. (ToolBox, 2017).

2.4 | Manual curation of reconstructed network

We performed a manual gene re-annotation of all metabolic genes present in the two draft reconstructions by individually inspecting and evaluating their presumptive metabolic functionality. We further verified these by BLASTp searches against the KEGG (Kanehisa & Goto, 2000) and UniProtKB/Swiss-Prot (Apweiler et al., 2004) databases. Associated reactions were collected and compared to those present in the draft reconstruction. These reactions were either directly found in the databases or, when available, from appropriate genome-scale reconstructions in the BiGG database (King et al., 2015). Any discrepancies were resolved through the addition or removal of reactions and/or associated genes.

As with iCY1170_DHA, the draft model accounted for three cell compartments: the extracellular space, the cytoplasm, and the mitochondria. Subcellular predictions were therefore made for all putative proteins using HECTAR (Gschloessl et al., 2008) and DeepLoc (Almagro Armenteros et al., 2017). In cases of differing predictions, HECTAR took precedence over DeepLoc as it is specifically tailored to predicting the subcellular targeting of proteins from the eukaryotic clade of heterokonts (Gschloessl et al., 2008; Leyland et al., 2017). We also performed qualitative evaluations in cases of conflicting predictions or when subcellular localization could be established from high-quality biochemical information. When subcellular localization of existing genes in the model was changed, appropriate transport reactions were added if subsections of the associated metabolic pathways now appeared in different compartments. We either found candidate transporter proteins directly from the genome annotation or by BLAST searches against the aforementioned databases, as well as in the Transporter Classification Database (TCDB) (Saier et al., 2016).

2.5 | Detection and removal of energy-generating cycles (EGCs)

To identify the presence of energy-generating cycles (EGCs), we added a set of energy dissipation reactions ξ and tested whether

these were able to carry a non-zero flux in a closed model (a listing is available in Table S2). Each dissipation reaction $e_i \in \xi$ was iteratively added to the reconstruction and subsequently selected as the objective function to be maximized in a closed model (i.e., all exchange reactions constrained to zero). This approach is described by the following linear program

$$\max e_i \quad (4)$$

$$\text{s. t. } \sum_{j=1}^n s_{ij} v_j = 0, \forall i \in M, \quad (5)$$

$$v_j^{lb} \leq v_j \leq v_j^{ub}, \forall j \in I, \quad (6)$$

$$v_k = 0, \forall k \in E, \quad (7)$$

where M is the set of metabolites, and I and E are the sets of internal and exchange reactions, respectively. In the case of a non-zero objective value, a reaction-deletion strategy was subsequently proposed in which a minimal subset of reactions to be deleted from these flux-carrying reactions was identified. A similar test was performed with only the uptake of the carbon source constrained to zero to account for alternative EGCs in which extracellular protons are taken up and used to drive the charging of energy carriers.

2.6 | Biomass reformulation

The biomass composition was adapted from the neutral lipid-free biomass (Shene et al., 2020). Splitting the biomass into preceding precursor reactions, we formulated unique biomass reactions of the following categories: proteins, carbohydrates, DNA, RNA, unsaponifiable matter, polar lipids, and free fatty acids. The relative molar content of each amino acid in proteins was assumed to be the same as that of *S. limacinum* SR21 (Ye, Qiao, et al., 2015). We also swapped each amino acid for their corresponding aminoacyl-tRNA and added additional energy carriers required for the process of translation. The total carbohydrate content was obtained from previous work (Shene et al., 2020), while the weight fractions was assumed to be the same as that of *S. limacinum* (Ye, Qiao, et al., 2015). To estimate the energy requirements for the polymerization of these monomeric carbohydrates, we employed their corresponding nucleotide sugars. As with the amino acids, we assumed that the molar abundance of each (deoxy)nucleotide in DNA and RNA was similar to that of *S. limacinum* (Ye, Qiao, et al., 2015). We also substituted the monomeric precursors with corresponding (deoxy)nucleoside triphosphates, simulating the energetic cost of replication and transcription, respectively. We used previously determined levels of unsaponifiable matter, polar lipids, and free fatty acids (Shene et al., 2020), while updating the fatty acyl distribution to that of T66 cells sampled during exponential growth. Lacking detailed experimental data on the quantitative levels of specific lipids of particular chain configurations, we further assumed that all lipid classes would have the same fractional acyl chain composition. We stoichiometrically weighted the components of each of the precursor reactions using appropriate correction factors and further scaled the

precursors in the final biomass reaction using experimentally determined weight fractions (i.e., g component gDW⁻¹) (Shene et al., 2020).

2.7 | Phenotypic growth predictions

To compare in vivo and model-predicted in silico growth rates, we performed two growth experiments separately using glucose and glycerol as the carbon sources, together with ammonium as a nitrogen source in both experiments. Cells were cultivated in 100 ml medium in 500 ml shaking flasks at 28°C and 250 rpm. Four samples of 10 ml were extracted during the exponential growth phase and subsequently centrifuged at 3200×g for 10 min. The supernatant was frozen to quantify the amount of the carbon source and ammonium. The pellet was washed once in 0.9% NaCl, and the resulting supernatant was carefully removed before drying at 105°C for 16–20 h to enable dry weight quantification. Glucose and glycerol were quantified by high-performance liquid chromatography (HPLC). Samples were centrifuged and filtered through 0.2 μm syringe filters before analyzed using an Aminex HPX-87-H column (BioRad Laboratories) at 45°C, and refractive index detection (RID-6A, Shimadzu). Five mmol H₂SO₄ was used as mobile phase at 0.6 ml/min. Ammonium quantities were determined using an enzymatic kit according to the manufacturer's instructions (Megazyme K-AMIA). Quantified levels of the carbon source and ammonium were subsequently used to estimate the specific substrate uptake rates.

3 | RESULTS

3.1 | Initial draft reconstruction

We initialized the reconstruction of the metabolic model by performing genome-wide bidirectional BLAST searches for orthologs between the template model proteins of *S. limacinum* SR21 and the predicted protein sequences of T66. In total, 995 candidate homologs were identified, which along with 1344 associated reactions and 1515 metabolites formed the basis of the draft reconstruction. In addition, 87 putative homologs were found using reciprocal protein-BLAST searches with less stringent alignment length cutoffs. We subsequently used the remaining set of template genes with no significant hits in tBLASTn searches against the genomic nucleotide sequence of T66 (available at GenBank; (Clark et al., 2016) under the accession number LNGJ00000000) to circumvent any insufficient genome coverage of the predicted protein sequences. A total of 30 additional candidate orthologs were identified, which along with the previous set of 87 proteins added 88 new metabolic reactions to the draft reconstruction. We also added all the unincorporated non-gene-associated transport and exchange reactions of the template model to the draft reconstruction. This was done to prevent their exclusion from impeding the ability of the model to generate necessary biomass precursors. At a later stage, we evaluated each of

these reactions individually and removed those that were unnecessary for a functional model.

To ensure that the model would be able to predict specific growth rates, we initiated a semi-automatic approach to identify and fill in the metabolic gaps necessary for biomass production. Due to insufficient knowledge of the particular biomass composition of T66, the biomass reaction of the template model was employed during these simulations (see "SupplInfo_Biomass_composition"). Although the primary goal was to enable the synthesis of biomass, we also introduced additional reactions to more accurately represent the metabolic network of T66. In total, we added 131 reactions during this procedure of which five were nonspontaneous gap-filling reactions with no identifiable candidate genes. Two additional gap-filling reactions were found as a minimal subset of reactions from iCY1170_DHA necessary for the synthesis of the biomass precursor L-galactose. These reactions were GDP mannose phosphorylase (EC:2.7.7.22) and GDP-L-galactose phosphorylase (EC:2.7.7.69). Interestingly, both of these gap-filling reactions had no associated genes in the template model, suggesting that their responsible enzymes might be elusive in thraustochytrids in general.

3.2 | Draft reconstruction from the KEGG database

To increase the predictive capabilities of the newly reconstructed model, we initiated comprehensive investigations of additional metabolic functionalities. To facilitate this process and aid in the identification of novel reactions and genes, we generated a secondary draft model from the KEGG database (Kanehisa & Goto, 2000) using the RAVEN Toolbox (Agren et al., 2013). The contents of this model, along with biochemical information available within the genome annotation were then used to identify reactions and genes that should be added to the draft reconstruction. We also identified candidate metabolic reactions through the inspection of metabolic dead-ends and associated blocked reactions of the model. Candidate genes for missing reactions were thereby identified and suitable metabolic reactions were collected, forming a repository of novel metabolic capability to be added to the draft reconstruction.

The secondary draft model harbored 1455 reactions, 1556 metabolites, and 1090 associated genes. Of these genes, 340 were unique to the KEGG model, while 404 genes were unique to the initial draft model. This highlights quite a substantial difference in genetic coverage between the two models and implies that the metabolic potential of both reconstructions might be inadequate. A similar discrepancy was found when studying the subsystem distributions of the model reactions in Figure 1. Although the number of reactions associated with each subsystem appear to be somewhat comparable, the sets of unique reactions make up a significant amount of all model reactions. In total, the initial draft reconstruction and the KEGG model each include 54.6% and 55.1% reactions that are not present in the other model. In the case of the draft reconstruction, these reactions were predominately associated

with the transport and exchange subsystems. While the KEGG database contains a comprehensive repository of high-quality biochemical information, it is not specifically tailored to assist in the reconstruction of GSMs. This is partly reflected in the absence of implemented transport reactions, which plays a key role in the genesis of genome-scale metabolic networks, particularly for the compartmentalized metabolism of eukaryotes. Associated with this is also information on the subcellular localization of proteins, which altogether is lacking in the model generated from KEGG.

3.3 | Manual curation

Motivated by the large metabolic disparity of the two reconstructions, we began a comprehensive model consolidation process. Here, the aim was to merge the two reconstructions while simultaneously performing manual curation on all the included model components. This entailed extensive gene re-annotation to enhance the accuracy of the gene-reaction associations, as well as assuring quality-control of the newly identified genes and associated reactions. Although highly laborious, the manual gene re-annotation proved to be a fruitful strategy. High-quality annotations on all 1191 genes of the final model were collected, strengthening the qualitative properties of the GSM and reinforcing the confidence in the included reactions compared with that of the automatically assembled draft reconstructions. The repository contains information on the presumed metabolic capabilities of all the metabolic genes, along with predicted subcellular localizations, bibliomic references of similar metabolic enzymes, and associated model reactions (see "SupplInfo_iVS1191_model_components", "A. Model genes"). When building this repository, we updated the gene rules for a substantial set of the model reactions. While, in many cases the associated reactions of a given gene were accurate according to the available biochemical information, the gene rules were frequently incorrect, often as a result of the exclusion of auxiliary subunits of both regulatory and catalytic activity. Their identification during the re-annotation allowed for more realistic gene-reaction associations, which will greatly increase the validity of future *in silico* analysis of gene essentiality, as well as the identification of realistic genetic engineering strategies.

We performed extensive validation of Enzyme Commission (EC) numbers as many of those included from the template reconstruction were either erroneous or originated from obsolete and/or outdated database entries. By using the MetaCyc (Kothari et al., 2013) database as a benchmark, we validated the metabolite formulas and charges of all model metabolites, as well as the reaction stoichiometries, reversibilities, and co-factor specificities. We further added reaction identifiers from KEGG (Kanehisa & Goto, 2000), BiGG (King et al., 2015), MetaCyc (Kothari et al., 2013), and MetaNetX (Ganter et al., 2013). Similarly for metabolites, we incorporated identifiers from the aforementioned database namespaces, as well as from ModelSEED (Henry et al., 2010), International Chemical Identifier (McNaught, 2008), Chemical Entities of Biological Interest

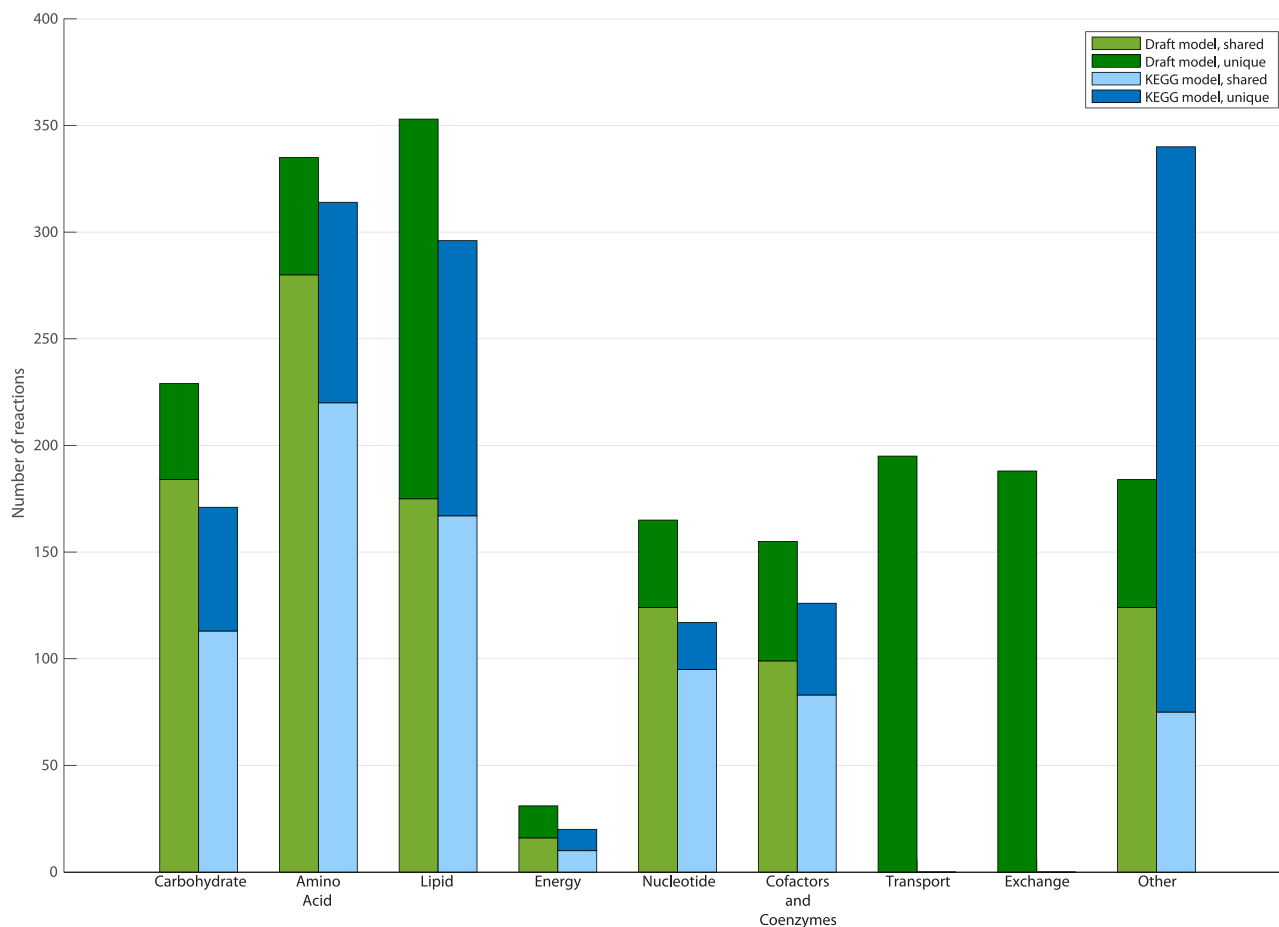


FIGURE 1 Subsystem distributions of the shared and unique reactions in the initial draft reconstruction of T66 and the KEGG model. The dissimilar number of shared reactions in each subsystem is a consequence of certain reactions of the draft reconstruction occurring in multiple compartments, or that a shared reaction are annotated to different subsystems in the two models. KEGG, Kyoto Encyclopedia of Genes and Genomes [Color figure can be viewed at wileyonlinelibrary.com]

(Degtyarenko et al., 2008), and Human Metabolome Database (Wishart et al., 2007).

Stoichiometric models of genome-scale metabolism may contain thermodynamically infeasible cycles which are able to charge intracellular energy carriers without any nutrient consumption (Fritzemeier et al., 2017). These cycles are products of inaccurate reversibilities of the constituent reactions, which often result from a lack of thermodynamic constraints. Of particular relevance are so-called EGCs, a subset of type II extreme pathways where the cycle drive the biochemical charging of metabolic energy carriers without any input of energy (Fritzemeier et al., 2017; Price et al., 2002). Following the iterative addition and subsequent maximization of the set of energy-dissipation reactions, it was revealed that the reconstructed model was able to charge all of the energy carriers without any input of reduced carbon. These thermodynamically infeasible cycles concertedly operated by taking up extracellular protons by means of a flux coupling between a proton-driven transport of a given metabolite and a reversible uniport reaction of the same compound. The set of reactions utilized this flow of protons to drive a continuous generation of cytosolic reducing power, which

subsequently was used to drive the biochemical charging of the other energy carriers. By inspecting the flux-carrying reactions, we disrupted all EGCs by performing appropriate reaction deletions.

3.4 | Resolving the biosynthetic pathway of PUFAs

In thraustochytrids, the biosynthesis of PUFAs primarily occurs by the action of a PKS enzymatic complex. Here, the acyl chains are covalently attached to the acyl-carrier protein (ACP) domain of the enzyme complex, which directs the moiety to the various catalytic domains during successive rounds of chain elongation (Ratledge, 2004). The PKS pathway from the template model followed a more simplistic mechanism where the associated biosynthetic steps were merged into generic reactions involving erroneous metabolic intermediates. In addition, the acyl moieties were present as acyl-CoA intermediates, thus omitting the final hydrolysis of the fatty acid from the ACP and subsequent condensation with CoA. We therefore implemented a more accurate representation of the PKS

TABLE 1 Candidate genes encoding the enzymatic subunits of the PKS complex responsible for the biosynthesis of PUFAs in T66

PKS subunit	Gene	Homologous gene	Sequence identity (%)
A	T66011701	KX651612.1	99.96
B	T66005413.1	KX651613.1	100
C	T66011702	KX651614.1	100
acpT	T66011703	KX651615.1	99.31

Note: The homologous genes are GenBank accession numbers of functionally characterized proteins of *Thraustochytrium* sp. 26185 (Meesapyodsuk & Qiu, 2016).

Abbreviations: PKS, polyketide synthase; PUFAs, polyunsaturated fatty acids.

pathway in which the acyl-CoA intermediates were replaced by acyl-ACPs. We added every single catalytic step as unique reactions to depict the presumed biochemical reaction mechanism occurring in vivo (Ratledge, 2004). We also implemented the final hydrolysis of the acyl chain in order for the model to predict more realistic energy demands due to the ensuing ATP-driven condensation with CoA. The updated PKS pathway contained a total of 81 unique metabolic reactions, with 75 associated acyl-ACP intermediates. The biosynthetic pathway was able to synthesize all of the PUFAs that T66 accumulates during lipid accumulation (Jakobsen et al., 2008). These consist of the two ω -3 fatty acids EPA (c20:5(n-3)) and DHA (c22:6(n-3)), and the ω -6 fatty acid docosapentaenoic acid (DPA, c22:5(n-6)). The resulting pathway thus diverges early on in the biosynthetic process by either retaining the unsaturated π -bond at the n-3 position, generating EPA and DHA, or reducing it, eventually producing DPA.

In iCY1170_DHA, 15 separate genes were present in the associated gene rules of the PKS pathway. However, upon further inspection it was revealed that many of these enzymes contained rather generic PKS domains, which did not seem to constitute either of the three catalytic subunits of the PKS complex. Through the process of manual gene re-annotation, we found three candidate genes in the genome of T66 which showed highly significant sequence similarity with the functionally characterized PUFA PKS subunits of *Thraustochytrium* sp. 26185 (Table 1) (Meesapyodsuk & Qiu, 2016). Along with an additional gene encoding the auxiliary phosphopantetheinyl transferase (acpT) subunit not present in iCY1170_DHA, we used these four genes to replace the previous set of 15 genes.

3.5 | Addition of a peroxisomal compartment

Due to its central role in lipid metabolism, it is necessary to incorporate a peroxisomal compartment to achieve a high-fidelity reconstructed network. Following extensive literature reviews and identification of proteins that were hypothesized to be localized in the peroxisome, we added a peroxisomal compartment to the reconstruction. This compartment harbors 135 unique reactions,

consisting of 92 internal and 43 transport reactions, respectively. Its metabolic capabilities are mainly associated with that of β -oxidation of fatty acids, along with the associated glyoxylate shunt, allowing for the gluconeogenic biosynthesis of carbohydrates from the acetyl-products of the β -oxidation pathway. The constituent reactions of the latter anaplerotic cycle were predicted to be localized to the peroxisome, as well as the cytosol and mitochondria, suggesting a rather complex interexchange of the metabolic intermediates between these compartments.

While the reactions associated with the glyoxylate shunt were present in iCY1170_DHA, thus allowing for growth on two-carbon compounds such as acetate, the model was unable to grow on any of its implemented fatty acids. This was caused by insufficient incorporation of necessary transport reactions and the erroneous subcellular localization of the mitochondrial electron-transferring-flavoprotein dehydrogenase (EC:1.5.5.1) to the cytosol, consequently preventing the mitochondrial degradation of these acyl chains. In addition, indispensable enzymatic steps required for the oxidation of unsaturated fatty acids, such as Δ^3 - Δ^2 -enoyl-CoA isomerase (EC:5.3.3.8) and 2,4-dienoyl-CoA reductase (EC:1.3.1.34), were also not implemented, thus preventing the metabolic network from being able to degrade the collection of fatty acids that it is able to synthesize. When the required reactions were added along with the peroxisomal compartment, the model was able to grow on all implemented fatty acids, as well as a set of volatile fatty acids reported to support growth of T66 cultures (Tables 2 and 3) (Jakobsen et al., 2007; Patel et al., 2020).

Based on available genomic data, the β -oxidation of fatty acids in T66 is situated in both the peroxisomal and mitochondrial compartment. However, the chain-length specificities of these two enzymatic machineries remain to be elucidated. We therefore made the

TABLE 2 Qualitative assessment of growth using the draft model, iVS1191, and iCY1170_DHA on various long to very-long chain fatty acids

Carbon source	Draft model ^a	iVS1191	iCY1170_DHA
Myristic acid, c14:0	-	+	-
Palmitic acid, c16:0	-	+	-
Palmitoleic acid, c16:1(n-7)	-	+	-
Stearic acid, c18:0	+	+	-
cis-Vaccenic acid, c18:1(n-7)	-	+	-
EPA, c20:5(n-3)	-	+	-
DPA, c22:5(n-6)	-	+	-
DHA, c22:6(n-3)	-	+	-

Note: Uptake rates of the carbon sources were arbitrarily set to 10 mmol gDW⁻¹ h⁻¹. Growth and nongrowth are denoted by + and -, respectively. Abbreviations: DHA, docosahexaenoic acid; DPA, docosapentaenoic acid; EPA, eicosapentaenoic acid.

^aDraft model following the initial gap filling to enable biomass production.

TABLE 3 Verification of growth predictions using the draft model and iVS1191 on a set of volatile fatty acids and a defined minimal glycerol/glutamate medium demonstrated to support growth of T66 *in vivo* (Jakobsen et al., 2007; Patel et al., 2020)

Carbon source	Draft model ^a	iVS1191	T66 <i>in vivo</i>
Formate, c1:0	-	+	+
Acetate, c2:0	+	+	+
Propanoate, c3:0	-	+	+
Butyrate, c4:0	-	+	+
Pentanoate, c5:0	-	+	+
Hexanoate, c6:0	-	+	+
Glycerol/glutamate ^b	+	+	+

Note: Uptake rates of the carbon sources were arbitrarily set to 10 mmol gDW⁻¹ h⁻¹. Growth and nongrowth are denoted by + and -, respectively. In the glycerol/glutamate simulation, cofactors and coenzymes were added to the biomass composition of the iVS1191 model to show that the model is also capable of synthesizing these with the required supplementation of thiamine and cobalamin as described in (Jakobsen et al., 2007) (see "SupplInfo_Biomass_composition" for the biomass compositions).

^aDraft model following the initial gap filling to enable biomass production.

^bGlutamate also serves as the N-source.

decision, similar to that of the GSM of *Phaeodactylum tricornutum* iLB1027 lipid (Levering et al., 2016), in which acyl chains of length 20 and more were assumed to initially be degraded solely in the peroxisomal compartment. The presumed end product octanoyl-CoA is then exported out of the peroxisome for further degradation in the mitochondrial β -oxidation pathway due to the presence of a peroxisomal carnitine O-octanoyltransferase (EC:2.3.1.137). The genuine substrate specificities of the two β -oxidation pathways are most likely overlapping. However, barring solid biochemical evidence of their acyl-chain preferences, we deem this differentiation the most probable based on the available genomic information.

3.6 | Cellular biomass reformulation

The biomass objective function is an abstract reaction in a GSM which contains the necessary biomolecular components to generate a unit of cellular dry weight (Feist & Palsson, 2010). By performing appropriate stoichiometric scaling of each biomass component, the flux through this reaction directly corresponds to the specific growth rate (h⁻¹) of the organism (Chan et al., 2017). Capturing the accurate macromolecular composition within the biomass reaction is therefore essential to correctly predict growth rates using a reconstructed GSM (Feist & Palsson, 2010). During the initial stages of the draft model construction and refinement, we used the biomass reaction of the template model iCY1170_DHA. However, the large content of lipids (43%, mainly TAGs) and carbohydrates (32%), and low content of proteins (12%), suggests a biomass deprived of nitrogenous compounds, presumably being closer to that of lipid accumulation

rather than exponentially growing cells. In strain T66, the lipid content of exponentially growing cells is merely 13%, not reaching the abovementioned levels until late in the lipid accumulation phase (Jakobsen et al., 2008). In addition, the most prevalent or only lipid class found in exponentially growing thraustochytrids with excess nitrogen are polar lipids (Aasen et al., 2016).

Consequently, we found it prudent to reformulate the biomass composition reaction using parts of the macromolecular composition data from a recently published GSM of the thraustochytrid strain *Oblongichytrium* sp. RT2316-13 (Shene et al., 2020). This biomass reaction is specifically tailored for exponentially growing cells where the lipid proportion is free of neutral lipids such as TAG, and predominately contains the polar lipids phosphatidylcholine and phosphatidylethanolamine. Additionally, the protein content has a more biologically realistic value of approximately 49%. Using an approach similar to that of previous studies (Levering et al., 2016), we added biomass-precursor reactions, each containing sets of molecules belonging to one of the particular categories: proteins, carbohydrates, DNA, RNA, unsaponifiable matter, polar lipids, and free fatty acids. We implicitly added growth-associated maintenance (GAM) requirements by choosing alternative biomass precursor metabolites and by adding associated polymerization costs (e.g., nucleoside triphosphates for RNA synthesis). We also constrained the non-growth associated maintenance (NGAM) reaction to 9.9 mmol gDW⁻¹ h⁻¹, assuming a linear relationship between the cultivation temperature and maintenance requirements using model-fitted values previously published (Shene et al., 2020). The biomass composition and detailed calculations are available in "SupplInfo_Biomass_composition."

3.7 | Final model reconstruction

The final model reconstruction iVS1191 contained a total of 1657 metabolites, 2095 reactions (1449 metabolic reactions, 415 transport reactions, and 232 exchange reactions), and 1191 associated genes. Each of these reactions are associated with 82 unique subsystems, which are subdivided into five individual compartments, one external extracellular compartment, as well as four internal compartments: the cytoplasm, the peroxisome, the mitochondria, and the mitochondrial intermembrane space. One of the most prominent changes from the template model iCY1170_DHA is the additional number of reactions, where the number of transport reactions shows the largest increase. The modest increase in the number of genes can be explained by the process of manual curation. Here, 233 genes from the draft model with subpar hits against enzymes of known functionalities was removed during the process. At the same time, 270 genes were added, either to replace those that were discarded, or as associated genes of novel metabolic reactions absent in iCY1170_DHA. Consequently, although the difference might seem insignificant, considerable alterations have been performed so as to more accurately reflect genuine biological organization with these gene-reaction associations.

TABLE 4 Comparison of features of the final model reconstruction iVS1191 and the two published thraustochytrid GSMs iCY1170_DHA and iCS1079

Features	iVS1191	iCY1170_DHA	iCS1079
Compartments	5	3	4
Genes	1191	1170	1079
Metabolites	1657	1659	1454
Reactions	2095	1769	1610
Metabolic	1448	1385	1352
Transport	415	195	178
Exchange	232	189	80
Blocked reactions	332	775	789
Dead-end/orphan metabolites	265	628	512
ORF coverage (%) ^a	10.2	7.9	7.3
MEMOTE score (%)	90	28	39

Note: The blocked reactions were identified by having minimal and maximal fluxes of zero when running flux variability analysis (FVA) on an open model (i.e., all exchange reactions left unconstrained). Dead-end and orphan metabolites were identified as metabolites unable to either be consumed or produced by the model. The ORF coverage was calculated by finding the fraction of protein-encoding genes in the model to the total number of predicted ORFs of the organism.

Abbreviations: DHA, docosahexaenoic acid; GSMs, genome-scale metabolic models; ORFs, open reading frames.

^aGenes found in the nucleotide genome sequence, but not as unique ORFs, were also included to account for insufficient coverage of the predicted protein sequences.

In addition to iCY1170_DHA, a revised GSM of *S. limacinum*, herein referred to as iCS1079, was recently published to simulate the growth and lipid phenotype of the closely related thraustochytrid strain *Oblongichytrium* sp. RT2316-13 using dynamic FBA (Shene et al., 2020). Here, the authors modified iCY1170_DHA by manually curating the model constituents and adding 220 new reactions to the reconstruction associated with amino acid, carbohydrate, and lipid metabolism. Using these previously reconstructed models, we compared their model components and properties with that of iVS1191. As presented in Table 4, iVS1191 shows a significant increase in metabolic coverage compared to both iCY1170_DHA and iCS1079. Specifically, we accomplished a considerable reduction in the number of blocked reactions and associated dead-end and orphan metabolites. In both iCY1170_DHA and iCS1079, a substantial subset of the reactions was unable to carry a non-zero flux under any condition, constituting around 44% and 49% of all model reactions, respectively. Similarly, around 38% and 35% of the metabolites were categorized as metabolic orphans or dead-ends, either only being consumed or produced by the models. Even with a substantial increase in the number of reactions in iVS1191, only around 16% of the reactions were found to be

blocked, while merely 16% of the metabolites were classified as metabolic orphans or dead-ends. This demonstrates how iVS1191 is able to utilize a greater subset of its metabolic capability, expectedly giving rise to more accurate phenotypic predictions.

While the open reading frame (ORF) coverage of iVS1191 did show a pronounced increase from that of iCY1170_DHA and iCS1079 (Table 4), this is most likely an effect of a smaller genome, and a corresponding reduction in the number of predicted ORFs. Whereas the genome size of *S. limacinum* is 60.93 Mb, with 14,859 unique ORFs (Institute, 2017), the genome size of T66 is merely 43 Mb, with a corresponding set of 11,683 predicted ORFs (Liu et al., 2016). Although this could imply a deficient genome coverage, it is comparable with other high-quality GSMs of the oleaginous species *Mortierella alpina* (Ye, Xu, et al., 2015) and *Yarrowia lipolytica* (Pan & Hua, 2012), each possessing an ORF coverage of 9.5% and 9.6%, respectively (Ye, Qiao, et al., 2015).

We also benchmarked iVS1191 against the open-source software suit MEMOTE (Lieven et al., 2020), which provides a collection of consensus model tests that evaluate key properties such as stoichiometry, annotation, biomass, and formal correctness of the model. When compared with the other thraustochytrid GSMs, iVS1191 showed major improvements in all test categories, obtaining a final score of 90% compared with 28% and 39% for iCY1170_DHA and iCS1079, respectively. Of particular importance was the considerable improvement in model consistency, which evaluates the extent of stoichiometric inconsistency, metabolic connectivity, and mass and charge balance. In this category, iVS1191 was awarded a score of 96%, while iCY1170_DHA and iCS1079 obtained a score of 64% and 87%, respectively.

3.8 | Phenotypic growth validation

A key part of the network evaluation stage is to compare model predictions with experimental data. Uncovered disparities might highlight deficiencies within the model reconstruction and further guide the modeler in subsequent reformulations and updates to close in on the gap between experimental and predicted phenotypes (Thiele & Palsson, 2010). To assess the quality of the constructed model, we first compared the predicted specific rate of biomass production against growth rates obtained from batch cultures of T66 on aerobic, minimal carbon-limited medium. We incorporated measured specific substrate uptake rates as lower bounds on the exchange reactions of the corresponding model metabolites and optimized growth by maximizing the biomass objective function using the standard FBA formulation of Equations (1)–(3). As presented in Table 5, the model-simulated growth-phenotypes were found to be highly consistent with the growth rates determined experimentally on both glucose and glycerol. The predicted growth on glucose showed a relative error of merely -1.6%, while the relative error of the simulated growth on glycerol was only 3.5%.

TABLE 5 Comparison of in vivo and in silico specific growth rates (h^{-1}) on aerobic carbon-limited minimal media, using measured carbon uptake fluxes ($\text{mmol gDW}^{-1} \text{h}^{-1}$) to constrain the metabolic model

	Minimal glucose	Minimal glycerol
Carbon uptake in vivo/in silico	1.440	2.440
Growth in vivo	0.124	0.114
Growth in silico	0.122	0.118
Ammonium uptake in vivo	1.110	0.990
Ammonium uptake in silico	0.981	0.953

Note: Growth rates were predicted by optimizing for biomass production.

4 | DISCUSSION

With this study, we present a successfully reconstructed high-quality GSM of the thraustochytrid strain *Aurantiochytrium* sp. T66 termed iVS1191. By complementing the use of automatic tools for model reconstruction with extensive and comprehensive manual curation, we considerably expanded the metabolic scope and coverage from that of the template reconstruction iCY1170_DHA. In doing so, the connectivity of the metabolic network showed drastic improvements when compared with this previously reconstructed GSM, as well as the recently published thraustochytrid model iCS1079, significantly reducing both the number of blocked reactions and associated dead-end and orphan metabolites. Model-driven analysis of growth demonstrated that iVS1191 could grow on all the fatty acids that it accumulates (Jakobsen et al., 2008), as well as a set of volatile fatty acids shown to enable growth in vivo (Patel et al., 2020), which both iCY1170_DHA and the draft reconstruction failed to utilize as single carbon sources (Tables 2 and 3). Understanding the role of this degradation of lipids and fatty acids during lipid accumulation is essential when trying to discern the metabolic properties of lipid production in thraustochytrids. The reconstructed model thus provides a highly valuable tool as a starting-point for model-driven generation of genetic engineering and cultivation strategies for increased DHA and lipid synthesis in T66.

During the model reconstruction process, we subjected the model to considerable manual curation and refinements. Particularly, we performed a genome-wide gene re-annotation of all the metabolic proteins of the two draft reconstructions. The motivation behind this labor-intensive re-annotation and comprehensive manual curation was threefold. First, during the manual gap filling procedure, as well as throughout the identification of novel metabolic capabilities, the quality of iCY1170_DHA was questioned due to the apparent scarcity of manual curation of the model reactions and associated genes. Several genes seemed to be annotated to erroneous sets of reactions, and the subcellular localization of a large number of reactions seemed to be based purely on automatic predictions. A telling example was the subcellular localization of the electron-transferring-flavoprotein dehydrogenase (EC:1.5.5.1), which transfers electrons from multiple

mitochondrial flavoprotein dehydrogenases, thus coupling the degradation of fatty acids and certain amino acids with oxidative phosphorylation (Watmough & Frerman, 2010). In iCY1170_DHA, this reaction was localized to the cytosol, effectively preventing the model from properly degrading these metabolites (see Table 2). Second, during the comparison between the genes of the initial draft model and the draft reconstruction from KEGG, considerable disparities in associated reactions were found between the genes that were present in both models. This was particularly true for proteins containing multiple catalytic domains, where the KEGG functionality in RAVEN appeared to have difficulties assigning appropriate KO IDs to these multifunctional enzymes. The quality of the reconciled draft models was therefore greatly assisted by this manual re-annotation and consolidation process. Last, inferring enzymatic activity from the genome annotation of T66 was in many cases rather challenging, primarily because of limited biochemical information in the annotation, but also due to occurrences of inaccurate assignments of database identifiers as well as associations with deprecated database entries.

Owing to this extensive curation of the individual model components, the stoichiometric consistency, metabolic connectivity, and mass and charge balance of the reconstruction exhibited drastic advancements. These curations allowed for the inclusion of a peroxisomal compartment, as well as a more realistic implementation of the PUFA-generating PKS pathway. Concurrent changes in the subcellular localization of key proteins associated with the β -oxidation of fatty acids enabled the model to grow on all its endogenously synthesized fatty acids, as well as multiple experimentally verified carbon sources (Table 3). Comparison of quantitative in vivo and in silico growth phenotypes also revealed the model able to accurately predict specific growth rates on both minimal glucose and glycerol media (Table 5), suggesting that the implemented biomass composition and associated ATP maintenance requirements are close to being representative of exponentially growing cells of T66. However, the predicted in silico ammonium uptake rates did show a larger deviance from the experimental values, particularly for growth on minimal glucose media in which the relative error was found to be -11.6% (Table 5). This indicates that the content of nitrogenous compounds of the biomass composition is somewhat insufficient, thus leading to a lower requirement for exogenously supplied ammonium. These results highlight the necessity for strain-specific and condition-dependent biomass compositions which in the future can be implemented with the reconstructed GSM to improve its predictive capabilities.

5 | CONCLUSION

We have developed and constructed a high-quality GSM of the thraustochytrid *Aurantiochytrium* sp. T66 termed iVS1191. The presented model provides the most comprehensive biochemical knowledgebase of any thraustochytrid to date, with a particular emphasis on lipid metabolism. Subjecting the model to large-scale manual curation, we significantly improved the metabolic coverage

and scope from that of previously published thraustochytrid GSMs. With a reformulated biomass composition, the model was able to accurately predict specific growth rates on minimal carbon media, as well as qualitatively reproduce growth phenotypes on multiple experimentally tested nutrient sources. We strongly believe that the reconstructed model will form a solid framework to explore and understand the metabolic properties of strain T66 and aid in the in silico generation of metabolic engineering and cultivation strategies for improved lipid and ω -3-PUFA productivities. In addition, the model encompasses a quality-controlled and quality-assured scaffold for future reconstructions of strain-specific thraustochytrid GSMs of great importance for biotechnological and industrial applications. Although the lack of a growth-coupled production of lipids in thraustochytrids hinders the use of many established frameworks for identifying genetic manipulation targets (Maia et al., 2016), other alternatives exist which could be a promising next step in the application of iVS1191 (Kim et al., 2019). Of particular interest is the method proposed by Kim et al. (2019) which uses the principle of minimization of metabolic adjustment to predict the flux distribution of nongrowing, lipid-accumulating cells, allowing for the discovery of metabolic engineering targets in *Y. lipolytica*. Due to the similar nature of lipid accumulation between thraustochytrids and oleaginous yeast, we believe that the use of this approach could be a fruitful first applications of the reconstruction.

ACKNOWLEDGMENTS

The authors would like to thank T. Kumelj and C. Schulz (Norwegian University of Science and Technology) for helpful discussions during the project, as well as S. Marcisauskas (Chalmers University of Technology) for assistance with RAVEN and the initial model reconstruction. We would also like to thank Inga Marie Aasen (SINTEF) for conducting the growth experiments of T66.

CONFLICT OF INTERESTS

The authors declare that there are no conflict of interests.

AUTHOR CONTRIBUTIONS

Eivind Almaas conceptualized the study. Vetle Simensen constructed, developed and curated the model, and performed all computational analyses, with input from Eivind Almaas and André Voigt. Vetle Simensen wrote the first version of the manuscript. Eivind Almaas and André Voigt oversaw the project and contributed to the final version of the manuscript. All authors have read and approved the final version of the manuscript.

DATA AVAILABILITY STATEMENT

The data that supports the findings of this study are available in the supplementary material of this article.

ORCID

Vetle Simensen  <http://orcid.org/0000-0002-2511-1052>

André Voigt  <http://orcid.org/0000-0002-3006-6970>

Eivind Almaas  <http://orcid.org/0000-0002-9125-326X>

REFERENCES

- Aasen, I. M., Ertesvåg, H., Heggset, T. M. B., Liu, B., Brautaset, T., Vadstein, O., & Ellingsen, T. E. (2016). Thraustochytrids as production organisms for docosahexaenoic acid (DHA), squalene, and carotenoids. *Applied Microbiology and Biotechnology*, 100(10), 4309–4321. <https://doi.org/10.1007/s00253-016-7498-4>
- Agren, R., Liu, L., Shoaie, S., Vongsangnak, W., Nookaew, I., & Nielsen, J. (2013). The RAVEN toolbox and its use for generating a genome-scale metabolic model for *Penicillium chrysogenum*. *PLoS Computational Biology*, 9(3), e1002980. <https://doi.org/10.1371/journal.pcbi.1002980>
- Almagro Armenteros, J. J., Sonderby, C. K., Sonderby, S. K., Nielsen, H., & Winther, O. (2017). DeepLoc: Prediction of protein subcellular localization using deep learning. *Bioinformatics*, 33(21), 3387–3395. <https://doi.org/10.1093/bioinformatics/btx431>
- Altschul, S. F., Gish, W., Miller, W., Myers, E. W., & Lipman, D. J. (1990). Basic local alignment search tool. *Journal of Molecular Biology*, 215(3), 403–410. [https://doi.org/10.1016/s0022-2836\(05\)80360-2](https://doi.org/10.1016/s0022-2836(05)80360-2)
- Apweiler, R., Bairoch, A., Wu, C. H., Barker, W. C., Boeckmann, B., Ferro, S., Gasteiger, E., Huang, H., Lopez, R., Magrane, M., Martin, M. J., Natale, D. A., O'Donovan, C., Redaschi, N., & Yeh, L. S. (2004). UniProt: The Universal Protein knowledgebase. *Nucleic Acids Res*, 32(Database issue), 32, D115–D119. <https://doi.org/10.1093/nar/gkh131>
- Beld, J., Lee, D. J., & Burkart, M. D. (2015). Fatty acid biosynthesis revisited: structure elucidation and metabolic engineering. *Molecular BioSystems*, 11(1), 38–59. <https://doi.org/10.1039/c4mb00443d>
- Bloomer, R. J., Larson, D. E., Fisher-Wellman, K. H., Galpin, A. J., & Schilling, B. K. (2009). Effect of eicosapentaenoic and docosahexaenoic acid on resting and exercise-induced inflammatory and oxidative stress biomarkers: A randomized, placebo controlled, cross-over study. *Lipids in Health and Disease*, 8, 36. <https://doi.org/10.1186/1476-511X-8-36>
- Bordbar, A., Monk, J. M., King, Z. A., & Palsson, B. O. (2014). Constraint-based models predict metabolic and associated cellular functions. *Nature Reviews Genetics*, 15(2), 107–120.
- Bouwens, M., van de Rest, O., Dellschaft, N., Bromhaar, M. G., de Groot, L. C., Geleijnse, J. M., Muller, M., & Afman, L. A. (2009). Fish-oil supplementation induces antiinflammatory gene expression profiles in human blood mononuclear cells. *American Journal of Clinical Nutrition*, 90(2), 415–424. <https://doi.org/10.3945/ajcn.2009.27680>
- Castañeda, M. T., Nuñez, S., Garelli, F., Voget, C., & De Battista, H. (2018). Comprehensive analysis of a metabolic model for lipid production in *Rhodospiridium toruloides*. *Journal of Biotechnology*, 280, 11–18. <https://doi.org/10.1016/j.jbiotec.2018.05.010>
- Chan, S. H. J., Cai, J., Wang, L., Simons-Senftle, M. N., & Maranas, C. D. (2017). Standardizing biomass reactions and ensuring complete mass balance in genome-scale metabolic models. *Bioinformatics*, 33(22), 3603–3609. <https://doi.org/10.1093/bioinformatics/btx453>
- Clark, K., Karsch-Mizrachi, I., Lipman, D. J., Ostell, J., & Sayers, E. W. (2016). GenBank. *Nucleic Acids Research*, 44(D1), D67–D72. <https://doi.org/10.1093/nar/gkv1276>
- Coletta, J. M., Bell, S. J., & Roman, A. S. (2010). Omega-3 Fatty acids and pregnancy. *Reviews in Obstetrics & Gynecology*, 3(4), 163–171.
- Degtyarenko, K., de Matos, P., Ennis, M., Hastings, J., Zbinden, M., McNaught, A., Alcántara, R., Darsow, M., Guedj, M., & Ashburner, M. (2008). ChEBI: A database and ontology for chemical entities of biological interest. *Nucleic Acids Research*, 36(Database issue), D344–D350. <https://doi.org/10.1093/nar/gkm791>
- Dias, O., Rocha, M., Ferreira, E. C., & Rocha, I. (2015). Reconstructing genome-scale metabolic models with merlin. *Nucleic Acids Research*, 43(8), 3899–3910. <https://doi.org/10.1093/nar/gkv294>
- Edgar, R., Domrachev, M., & Lash, A. E. (2002). Gene expression omnibus: NCBI gene expression and hybridization array data repository.

- Nucleic Acids Research*, 30(1), 207–210. <https://doi.org/10.1093/nar/30.1.207>
- El-Moselhy, K. M., Othman, A. I., Abd El-Azem, H., & El-Metwally, M. E. A. (2014). Bioaccumulation of heavy metals in some tissues of fish in the Red Sea, Egypt. *Egyptian Journal of Basic and Applied Sciences*, 1(2), 97–105. <https://doi.org/10.1016/j.ejbas.2014.06.001>
- Feist, A. M., & Palsson, B. O. (2010). The biomass objective function. *Current Opinion in Microbiology*, 13(3), 344–349. <https://doi.org/10.1016/j.mib.2010.03.003>
- Food and Agriculture Organization of the United Nations. (2018). The State of World Fisheries and Aquaculture 2018 - Meeting the sustainable development goals. <http://www.fao.org/3/i9540en/i9540EN.pdf>
- Fritzemeier, C. J., Hartleb, D., Szappanos, B., Papp, B., & Lercher, M. J. (2017). Erroneous energy-generating cycles in published genome scale metabolic networks: Identification and removal. *PLoS Computational Biology*, 13(4), e1005494. <https://doi.org/10.1371/journal.pcbi.1005494>
- Ganter, M., Bernard, T., Moretti, S., Stelling, J., & Pagni, M. (2013). MetaNetX.org: A website and repository for accessing, analysing and manipulating metabolic networks. *Bioinformatics*, 29(6), 815–816. <https://doi.org/10.1093/bioinformatics/btt036>
- Gschloessl, B., Guermeur, Y., & Cock, J. M. (2008). HECTAR: A method to predict subcellular targeting in heterokonts. *BMC Bioinformatics*, 9, 393. <https://doi.org/10.1186/1471-2105-9-393>
- Gu, C., Kim, G. B., Kim, W. J., Kim, H. U., & Lee, S. Y. (2019). Current status and applications of genome-scale metabolic models. *Genome Biology*, 20(1), 121. <https://doi.org/10.1186/s13059-019-1730-3>
- Gurobi Optimization, L. L. C. (2020). Gurobi optimizer reference manual. <http://www.gurobi.com>
- Heirendt, L., Arreckx, S., Pfau, T., Mendoza, S. N., Richelle, A., Heinken, A., Haraldsdóttir, H. S., Wachowiak, J., Keating, S. M., Vlasov, V., Magnusdóttir, S., Ng, C. Y., Preciat, G., Žagare, A., Chan, S. H. J., Aurich, M. K., Clancy, C. M., Modamio, J., Sauls, J. T., ... Fleming, R. M. T. (2019). Creation and analysis of biochemical constraint-based models using the COBRA Toolbox v.3.0. *Nature Protocols*, 14(3), 639–702. <https://doi.org/10.1038/s41596-018-0098-2>
- Henry, C. S., DeJongh, M., Best, A. A., Frybarger, P. M., Lindsay, B., & Stevens, R. L. (2010). High-throughput generation, optimization and analysis of genome-scale metabolic models. *Nature Biotechnology*, 28(9), 977–982. <https://doi.org/10.1038/nbt.1672>
- Hosomi, R., Yoshida, M., & Fukunaga, K. (2012). Seafood consumption and components for health. *Global Journal of Health Science*, 4(3), 72–86. <https://doi.org/10.5539/gjhs.v4n3p72>
- Huang, T. Y., Lu, W. C., & Chu, I. M. (2012). A fermentation strategy for producing docosahexaenoic acid in *Aurantiochytrium limacinum* SR21 and increasing C22:6 proportions in total fatty acid. *Bioresource Technology*, 123, 8–14. <https://doi.org/10.1016/j.biortech.2012.07.068>
- Institute, J. G. (2017). JGI Aurl1. <https://genome.jgi.doe.gov/-Aurl1/Aurl1.home.html>
- Jakobsen, A. N., Aasen, I. M., Josefsen, K. D., & Strom, A. R. (2008). Accumulation of docosahexaenoic acid-rich lipid in thraustochytrid *Aurantiochytrium* sp. strain T66: Effects of N and P starvation and O₂ limitation. *Applied Microbiology and Biotechnology*, 80(2), 297–306. <https://doi.org/10.1007/s00253-008-1537-8>
- Jakobsen, A. N., Aasen, I. M., & Strøm, A. R. (2007). Endogenously synthesized (–)-proto-quercitol and glycine betaine are principal compatible solutes of *Schizochytrium* sp. strain S8 (ATCC 20889) and three new isolates of phylogenetically related thraustochytrids. *Applied and Environmental Microbiology*, 73(18), 5848–5856. <https://doi.org/10.1128/AEM.00610-07>
- Kanehisa, M., & Goto, S. (2000). KEGG: kyoto encyclopedia of genes and genomes. *Nucleic Acids Research*, 28(1), 27–30. <https://doi.org/10.1093/nar/28.1.27>
- Karp, P. D., Latendresse, M., Paley, S. M., Krummenacker, M., Ong, Q. D., Billington, R., Kothari, A., Weaver, D., Lee, T., Subhraveti, P., Spaulding, A., Fulcher, C., Keseler, I. M., & Caspi, R. (2016). Pathway Tools version 19.0 update: software for pathway/genome informatics and systems biology. *Briefings in Bioinformatics*, 17(5), 877–890. <https://doi.org/10.1093/bib/bbv079>
- Kim, M., Park, B. G., Kim, E.-J., Kim, J., & Kim, B.-G. (2019). In silico identification of metabolic engineering strategies for improved lipid production in *Yarrowia lipolytica* by genome-scale metabolic modeling. *Biotechnology for Biofuels*, 12(1), 187. <https://doi.org/10.1186/s13068-019-1518-4>
- King, Z. A., Lu, J., Dräger, A., Miller, P., Federowicz, S., Lerman, J. A., Ebrahim, A., Palsson, B. O., & Lewis, N. E. (2015). BiGG Models: A platform for integrating, standardizing and sharing genome-scale models. *Nucleic Acids Research*, 44(D1), D515–D522. <https://doi.org/10.1093/nar/gkv1049>
- Kothari, A., Kubo, A., Fulcher, C. A., Weaver, D. S., Weerasinghe, D., Foerster, H., Keseler, I. M., Dreher, K., Mueller, L. A., Latendresse, M., Krummenacker, M., Subhraveti, P., Zhang, P., Ong, Q., Billington, R., Caspi, R., Paley, S., Holland, T. A., Altman, T., & Karp, P. D. (2013). The MetaCyc database of metabolic pathways and enzymes and the BioCyc collection of Pathway/Genome Databases. *Nucleic Acids Research*, 42(D1), D459–D471. <https://doi.org/10.1093/nar/gkt1103>
- Lauritzen, L., Brambilla, P., Mazzocchi, A., Harsløf, L. B. S., Ciappolino, V., & Agostoni, C. (2016). DHA effects in brain development and function. *Nutrients*, 8(1), 6. <https://doi.org/10.3390/nu8010006>
- Levering, J., Broddrick, J., Dupont, C. L., Peers, G., Beerli, K., Mayers, J., Gallina, A. A., Allen, A. E., Palsson, B. O., & Zengler, K. (2016). Genome-scale model reveals metabolic basis of biomass partitioning in a model diatom. *PLoS One*, 11(5), e0155038. <https://doi.org/10.1371/journal.pone.0155038>
- Levering, J., Broddrick, J., & Zengler, K. (2015). Engineering of oleaginous organisms for lipid production. *Current Opinion in Biotechnology*, 36, 32–39. <https://doi.org/10.1016/j.copbio.2015.08.001>
- Leyland, B., Leu, S., & Boussiba, S. (2017). Are thraustochytrids algae? *Fungal Biology*, 121(10), 835–840. <https://doi.org/10.1016/j.funbio.2017.07.006>
- Li, J., Liu, R., Chang, G., Li, X., Chang, M., Liu, Y., Jin, Q., & Wang, X. (2015). A strategy for the highly efficient production of docosahexaenoic acid by *Aurantiochytrium limacinum* SR21 using glucose and glycerol as the mixed carbon sources. *Bioresource Technology*, 177, 51–57. <https://doi.org/10.1016/j.biortech.2014.11.046>
- Lieven, C., Beber, M. E., Olivier, B. G., Bergmann, F. T., Ataman, M., Babaei, P., Bartell, J. A., Blank, L. M., Chauhan, S., Correia, K., Diener, C., Dräger, A., Ebert, B. E., Edirisinghe, J. N., Faria, J. P., Feist, A. M., Fengos, G., Fleming, R. M. T., García-Jiménez, B., ... Zhang, C. (2020). MEMOTE for standardized genome-scale metabolic model testing. *Nature Biotechnology*, 38(3), 272–276. <https://doi.org/10.1038/s41587-020-0446-y>
- Liu, B., Ertesvåg, H., Aasen, I. M., Vadstein, O., Brautaset, T., & Heggeset, T. M. B. (2016). Draft genome sequence of the docosahexaenoic acid producing thraustochytrid *Aurantiochytrium* sp. T66. *Genomics Data*, 8, 115–116. <https://doi.org/10.1016/j.gdata.2016.04.013>
- Loira, N., Dulermo, T., Nicaud, J.-M., & Sherman, D. J. (2012). A genome-scale metabolic model of the lipid-accumulating yeast *Yarrowia lipolytica*. *BMC Systems Biology*, 6(1), 35. <https://doi.org/10.1186/1752-0509-6-35>
- Machado, D., Andrejev, S., Tramontano, M., & Patil, K. R. (2018). Fast automated reconstruction of genome-scale metabolic models for microbial species and communities. *Nucleic Acids Research*, 46(15), 7542–7553. <https://doi.org/10.1093/nar/gky537>
- Maia, P., Rocha, M., & Rocha, I. (2016). In silico constraint-based strain optimization methods: The Quest for optimal cell factories.

- Microbiology and Molecular Biology Reviews*, 80(1), 45–67. <https://doi.org/10.1128/MMBR.00014-15>
- Martyushenko, N., & Almaas, E. (2019). ModelExplorer: Software for visual inspection and inconsistency correction of genome-scale metabolic reconstructions. *BMC Bioinformatics*, 20(1), 56. <https://doi.org/10.1186/s12859-019-2615-x>
- MATLAB. (2019). version 9.7.0 (2019b). The MathWorks Inc.
- McNaught, A. (2008). The IUPAC International Chemical Identifier: InChI. Meesapyodsuk, D., & Qiu, X. (2016). Biosynthetic mechanism of very long chain polyunsaturated fatty acids in *Thraustochytrium* sp. 26185. *Journal of Lipid Research*, 57(10), 1854–1864. <https://doi.org/10.1194/jlr.M070136>
- Mendoza, S. N., Olivier, B. G., Molenaar, D., & Teusink, B. (2019). A systematic assessment of current genome-scale metabolic reconstruction tools. *Genome Biology*, 20(1), 158. <https://doi.org/10.1186/s13059-019-1769-1>
- Metz, J. G., Roessler, P., Facciotti, D., Levering, C., Dittrich, F., Lassner, M., Valentine, R., Lardizabal, K., Domergue, F., Yamada, A., Yazawa, K., Knauf, V., & Browse, J. (2001). Production of polyunsaturated fatty acids by polyketide synthases in both prokaryotes and eukaryotes. *Science*, 293(5528), 290–293. <https://doi.org/10.1126/science.1059593>
- Mishra, P., Park, G.-Y., Lakshmanan, M., Lee, H.-S., Lee, H., Chang, M. W., Ching, C. B., Ahn, J., & Lee, D.-Y. (2016). Genome-scale metabolic modeling and in silico analysis of lipid accumulating yeast *Candida tropicalis* for dicarboxylic acid production. *Biotechnology and Bioengineering*, 113(9), 1993–2004. <https://doi.org/10.1002/bit.25955>
- O'Brien, E. J., Monk, J. M., & Palsson, B. O. (2015). Using genome-scale models to predict biological capabilities. *Cell*, 161(5), 971–987. <https://doi.org/10.1016/j.cell.2015.05.019>
- Orth, J. D., Thiele, I., & Palsson, B. O. (2010). What is flux balance analysis? *Nature Biotechnology*, 28(3), 245–248. <https://doi.org/10.1038/nbt.1614>
- Pan, P., & Hua, Q. (2012). Reconstruction and in silico analysis of metabolic network for an oleaginous yeast, *Yarrowia lipolytica*. *PLoS One*, 7(12), 1–11. <https://doi.org/10.1371/journal.pone.0051535>
- Patel, A., Rova, U., Christakopoulos, P., & Matsakas, L. (2020). Assessment of fatty acids profile and omega-3 polyunsaturated fatty acid production by the oleaginous marine thraustochytrid *Aurantiochytrium* sp. T66 cultivated on volatile fatty acids. *Biomolecules*, 10(5), 694. <https://doi.org/10.3390/biom10050694>
- Pitkänen, E., Jouhten, P., Hou, J., Syed, M. F., Blomberg, P., Kludas, J., Oja, M., Holm, L., Penttilä, M., Rousu, J., & Arvas, M. (2014). Comparative genome-scale reconstruction of gapless metabolic networks for present and ancestral species. *PLoS Computational Biology*, 10(2), e1003465. <https://doi.org/10.1371/journal.pcbi.1003465>
- Price, N. D., Famili, I., Beard, D. A., & Palsson, B. O. (2002). Extreme pathways and Kirchhoff's second law. *Biophysical Journal*, 83(5), 2879–2882. [https://doi.org/10.1016/s0006-3495\(02\)75297-1](https://doi.org/10.1016/s0006-3495(02)75297-1)
- Ratledge, C. (2004). Fatty acid biosynthesis in microorganisms being used for single cell oil production. *Biochimie*, 86(11), 807–815. <https://doi.org/10.1016/j.biochi.2004.09.017>
- Rawn, D. F., Forsyth, D. S., Ryan, J. J., Breakell, K., Verigin, V., Nicolidakis, H., Hayward, S., Laffey, P., & Conacher, H. B. (2006). PCB, PCDD and PCDF residues in fin and non-fin fish products from the Canadian retail market 2002. *Science of the Total Environment*, 359(1–3), 101–110. <https://doi.org/10.1016/j.scitotenv.2005.04.021>
- Saier, M. H. J., Reddy, V. S., Tsu, B. V., Ahmed, M., S., Li, C., & Moreno-Hagelsieb, G. (2016). The transporter classification database (TCDB): Recent advances. *Nucleic Acids Research*, 44(D1), D372–D379. <https://doi.org/10.1093/nar/gkv1103>
- Shene, C., Paredes, P., Flores, L., Leyton, A., Asenjo, J. A., & Chisti, Y. (2020). Dynamic flux balance analysis of biomass and lipid production by Antarctic thraustochytrid *Oblongichytrium* sp. RT2316-13. *Biotechnology and Bioengineering*, 117, 3006–3017. <https://doi.org/10.1002/bit.27463>
- Swanson, D., Block, R., & Mousa, S. A. (2012). Omega-3 fatty acids EPA and DHA: Health benefits throughout life. *Advances in Nutrition* 3(1), 1–7. <https://doi.org/10.3945/an.111.000893>
- Thiele, I., & Palsson, B. O. (2010). A protocol for generating a high-quality genome-scale metabolic reconstruction. *Nature Protocols*, 5(1), 93–121. <https://doi.org/10.1038/nprot.2009.203>
- Tibocha-Bonilla, J. D., Zuñiga, C., Godoy-Silva, R. D., & Zengler, K. (2018). Advances in metabolic modeling of oleaginous microalgae. *Biotechnology for Biofuels*, 11(1), 241. <https://doi.org/10.1186/s13068-018-1244-3>
- Tiukova, I. A., Prigent, S., Nielsen, J., Sandgren, M., & Kerkhoven, E. J. (2019). Genome-scale model of *Rhodotorula toruloides* metabolism. *Biotechnology and Bioengineering*, 116(12), 3396–3408. <https://doi.org/10.1002/bit.27162>
- ToolBox, B. (2017). Pre-trained HMM, Eukaryota, Identity 100%. <http://biomet-toolbox.chalmers.se/index.php?page=downtools-raven>
- Vongsangnak, W., Ruenwai, R., Tang, X., Hu, X., Zhang, H., Shen, B., Song, Y., & Laoteng, K. (2013). Genome-scale analysis of the metabolic networks of oleaginous *Zygomycete* fungi. *Gene*, 521(1), 180–190. <https://doi.org/10.1016/j.gene.2013.03.012>
- Watmough, N. J., & Frerman, F. E. (2010). The electron transfer flavoprotein: ubiquinone oxidoreductases. *Biochimica et Biophysica Acta/General Subjects*, 1797(12), 1910–1916. <https://doi.org/10.1016/j.bbabi.2010.10.007>
- Wishart, D. S., Tzur, D., Knox, C., Eisner, R., Guo, A. C., Young, N., Cheng, D., Jewell, K., Arndt, D., Sawhney, S., Fung, C., Nikolai, L., Lewis, M., Coutouly, M.-A., Forsythe, I., Tang, P., Shrivastava, S., Jeroncic, K., Stothard, P., ... Querengesser, L. (2007). HMDB: The Human Metabolome Database. *Nucleic Acids Research*, 35(Database issue), 35 D521–D526. <https://doi.org/10.1093/nar/gkl923>
- Ye, C., Qiao, W., Yu, X., Ji, X., Huang, H., Collier, J. L., & Liu, L. (2015). Reconstruction and analysis of the genome-scale metabolic model of *Schizochytrium limacinum* SR21 for docosahexaenoic acid production. *BMC Genomics*, 16, 799. <https://doi.org/10.1186/s12864-015-2042-y>
- Ye, C., Xu, N., Chen, H., Chen, Y. Q., Chen, W., & Liu, L. (2015). Reconstruction and analysis of a genome-scale metabolic model of the oleaginous fungus *Mortierella alpina*. *BMC Systems Biology*, 9, 1. <https://doi.org/10.1186/s12918-014-0137-8>

SUPPORTING INFORMATION

Additional Supporting Information may be found online in the supporting information tab for this article.

How to cite this article: Simensen V., Voigt A., & Almaas E. High-quality genome-scale metabolic model of *Aurantiochytrium* sp. T66. *Biotechnology and Bioengineering*. 2021;118:2105–2117. <https://doi.org/10.1002/bit.27726>